I&EC research
Industrial & Engineering Chemistry Research

ACS Editors' Choice

Article

pubs.acs.org/IECR

Terms of Use

Synthesis of Alumina-Modified Cigarette Soot Carbon As an Adsorbent for Efficient Arsenate Removal

He Chen,[†,‡] Jiaxing Li,*[,†,‡] Xilin Wu,[‡] and Xiangke Wang[†,§]

[†]School of Environment and Chemical Engineering, North China Electric Power University, Beijing 102206, P.R. China

[‡]Key Laboratory of Novel Thin Film Solar Cells, Institute of Plasma Physics, Chinese Academy of Sciences, P.O. Box 1126, 230031 Hefei, PR China

[§]Faculty of Engineering, King Abdulaziz University, Jeddah 21589, Saudi Arabia

Supporting Information

ABSTRACT: In this study, the alumina (Al_2O_3) modified cigarette soot carbon (CSC) (Al_2O_3/CSC) were fabricated via a simple one-step thermal method using CSC as template. The as-synthesized Al_2O_3/CSC were used as adsorbents for efficient arsenate (As(V)) elimination. Different weight ratios of Al_2O_3/CSC (Al_2O_3:CSC = 1:1, 2:1, and 3:1) were fabricated, and the corresponding As(V) removal performance revealed that the synthesized $2Al_2O_3$/CSC (mass ratio) possessed the best separation property and the highest adsorption capacity. A natural groundwater sample collected from Togtoh county, Inner Mongolia (China), with an initial concentration of 233 μg/L As(V) was applied to test the $2Al_2O_3$/CSC application in actual groundwater purification. After processing with $2Al_2O_3$/CSC, the As(V) concentration was reduced to 8.0 μg/L, which met the quality standard of World Health Organization (WHO). A regeneration test indicated that the $2Al_2O_3$/CSC could be reused for at least six times without significant decrease in the adsorption capacity. The as-synthesized $2Al_2O_3$/CSC with the maximum removal capacity of 96.9 mg/g for As(V) would be a promising material for the efficient removal of As(V) from groundwater with high As(V) concentrations in actual applications.

1. INTRODUCTION

Excessive arsenic (As) compounds in drinking water, which may cause skin alteration and many types of cancers, is a severe threat to human health.[1,2] The formation of arsenic pollution could be attributed to natural processes and human activity.[3] Unfortunately, groundwater, a main source of drinking water, tends to be polluted by both routes. Growing areas of groundwater worldwide, in Argentina, China, Chile, Hungary, and Mexico, are detected to be high-level arsenic contaminated.[4] In the Pannonian Basin (Central Europe), the arsenic concentration has reached 210 μg/L.[5] As an acute problem to be resolved, arsenic contaminated water has gradually gained worldwide attention. The safety arsenic concentration in drinking water has been reduced from 50 to 10 μg/L by the World Health Organization (WHO)[6] and the EU drinking-water directive. To guarantee the safety of human health, new technologies and materials are required to eliminate excessive arsenic in groundwater.

Various technologies, such as coagulation/filtration, chemical precipitation, ion-exchange, and adsorption, are applied to remove arsenic from drinking water. Since most of the arsenic contaminated regions are located in developing countries, especially in rural areas, simple and low-cost methods are required due to economic considerations. However, most methods mentioned above fail to meet this requirement. For example, reverse osmosis membrane devices are relatively expensive, requiring electric power and skilled technicians to operate, which make them unsuitable for common users. For coagulation/filtration, the inconvenience of sludge disposal and difficulty of floc separation greatly limit domestic applications. In the case of ion-exchange techniques, the high cost and logistic constraints become restrictions for this type of application.[7]

Adsorption is generally regarded as an attractive method for its low cost and simple operation. In the quest for easily accessible, low-price, and effective adsorbents, natural materials and byproducts from industries and agriculture have been recognized as a valuable resource.[8] Different biomaterials including banana peels,[9] beer brewery waste,[10] rice hull ash,[11] sonochemical treated fly ash,[12] agar,[13] etc., have been tested as adsorbents to eliminate environmental pollutants from aqueous solutions. To uptake negative charged As(V) anions from aqueous solutions, the biomaterials were supposed to be modified with metal oxides, such as Fe_2O_3 and CuO.[7,14] In recent reports, the metal-based materials exhibited marvelous adsorption performance to arsenate in aqueous solution.[15−18] However, in most thermal treatment processes, metal oxides just formed on the outer-surface of the support materials and inner spaces were not utilized, which greatly restricted the best adsorption performance.

As one of the world's largest nonfood cash crops, tobacco is extensively grown in China, Brazil, India, USA, etc. Millions of cigarettes are produced everyday, which generates carbon monoxide, nicotine, and other harmful gas to human body after smoking. When people smoke, incomplete combustion emerges as air is sucked through the tobacco within a short time. Thus, a certain amount of activated carbon is formed and

Received: July 31, 2014
Revised: September 15, 2014
Accepted: September 19, 2014
Published: September 19, 2014

   dx.doi.org/10.1021/ie503057g | *Ind. Eng. Chem. Res.* 2014, 53, 16051−16060

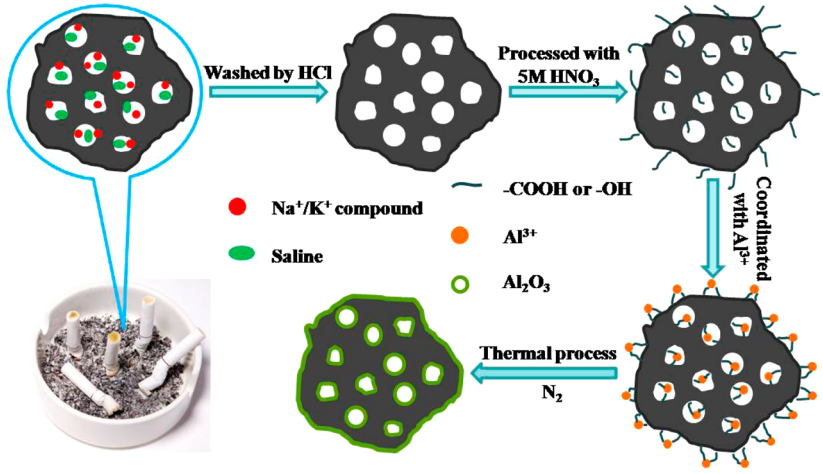

Figure 1. Proposed mechanism for the formation of Al_2O_3-modified CSC.

incorporated in the cigarette soot. In this work, cigarette soot carbon (CSC), the burning waste which possesses natural porous structure, was collected and reused as a template for the uptake of As(V) from aqueous solutions. Different from the artificial template, the CSC possesses the merits of easy-accessibility and low-price. In previous reports, some carbon materials from old tree leaves and rice hull were applied as templates for water purification;[11,17] however, these raw materials require further thermal treatment, which is energy wasted. To achieve an ideal adsorption performance, Al_2O_3, an environmental friendly and extensively studied material for As(V) removal,[14,19] was loaded on the surface of cigarette soot carbon. Due to the production process and high surface energy, nanosized Al_2O_3 particles are apt to form aggregations, which is unfavorable for water cleanup.[20] Besides, traditional Al_2O_3 materials tend to form gels in aqueous solutions and could not be separated completely in a short time without centrifugation. These demerits could be significantly reduced by the synthesized microscale Al_2O_3/CSC. The Al_2O_3/CSC was fabricated through a simple one-step thermal method. To simulate the practical adsorption situation, NaCl is added to the experimental system as the impurities.

In this study, a modified method was applied to evaluate CSC and Al_2O_3-modified CSC whether they can remove arsenate from water. The impact factors, such as pH, temperature, and mass ratios, on As(V) removal by the as-synthesized Al_2O_3/CSC were studied. To achieve a better understanding of the As(V) adsorption on Al_2O_3/CSC, FT-IR and XPS techniques were utilized to explore the possible adsorption mechanism. The reuse of CSC and the high removal efficiency of As(V) ions on the Al_2O_3/CSC may provide a referential study to groundwater or wastewater cleanup and peer's work.

2. EXPERIMENTAL SECTION

2.1. Materials. All chemicals were purchased from Sigma-Aldrich as reagent grade and used directly without further purification. Milli-Q water (Millipore, Billerica, MA, USA) was used to prepare the As(V) stock solution and used in all the experiments.

2.2. Synthetic Method. About 2.0 g cigarette soot was pretreated with 20 mL concentrated HCl to estimate the saline and metal ions (see the Supporting Information, Figure S1). About 0.74 g CSC was retrieved, and the mass ratio of CSC/CS was 37%, accordingly. To achieve an ideal hydrophilic effect, the CSC was then mixed with 20 mL 5.0 mol/L HNO_3 and the suspension was placed in 80 °C water bath for 4 h under continuous agitation. The solid samples were washed several times by Milli-Q water and vacuum-dried at 70 °C overnight. The precursors of Al_2O_3/CSC were prepared by adding 1.0 g CSC powder into 100 mL 0.286, 0.571, and 0.857 mol/L $Al(NO_3)_3$ solutions, which corresponded to Al_2O_3/CSC mass ratios of 1:1, 2:1, and 3:1, respectively, under gentle agitation.[20] Then, the precursors were separated and vacuum-dried at 70 °C overnight, which was subsequently calcined at 800 °C in N_2 at a heating rate of 5 °C/min, and kept at 800 °C for 120 min. The obtained Al_2O_3/CSC was ground into fine powders after cooling, and the synthetic mechanism is shown in Figure. 1. In the experiment, γ-Al_2O_3 powder (Aluminum Oxide C, purity of 99.6%) was used for comparison.

2.3. Characterization. The CSC and Al_2O_3/CSC were characterized by energy dispersive spectrometer (EDS), scanning electron microscopy (SEM), transmission electron microscopy (TEM), Barrett−Emmett−Teller specific area (BET), Fourier transform infrared spectroscopy (FT-IR), X-ray diffraction (XRD), and X-ray photoelectron spectroscopy (XPS). The SEM images were obtained with a JEOL JSM-6330F operated at the beam energy of 15.0 kV. TEM images were performed on a JEOL-2010 TEM with an accelerating voltage of 200 kV. The BET specific area test was performed on a Micromeritics ASAP 2010 system at 77 K. FT-IR spectra were performed on a Nicolet Magana-IR 750 spectrometer over a wavenumber range from 400 to 4000 cm^{-1}. The XRD measurements over an angle range of 10−70° were conducted on a Philips X'Pert Pro Super X-ray diffract meter equipped with a Cu Kα source (λ = 1.54178 Å). The XPS analyses were carried out in a VG Scientific ESCALAB Mark II spectrometer equipped with two ultrahigh vacuum (UHV) chambers.

2.4. Batch Adsorption Experiments. Adsorption experiments of As(V) on the as-synthesized Al_2O_3/CSC were conducted in 0.01 mol/L NaCl solutions in 10 mL polyethylene test tubes. Specifically, 0.12 g Al_2O_3/CSC powders were dispersed in 100 mL Milli-Q water to achieve a 1.2 g/L stock adsorbent concentration. The As(V) solution, NaCl solution, Al_2O_3/CSC stock suspension, and Milli-Q water were added in the 10 mL polyethylene test tubes respectively to achieve the desired concentrations of different components.[21,22] A negligible amount of HCl or NaOH solution was added to

dx.doi.org/10.1021/ie503057g | Ind. Eng. Chem. Res. 2014, 53, 16051−16060

the suspensions to achieve the desired pH values. The tubes were placed in an oscillator, after gentle shaking for 24 h, adsorption equilibrium was achieved and the solid phases were separated from the suspension by centrifugation at 9000 rpm for 10 min. As(V) concentrations in the supernatants were detected by graphite furnace atomic absorption spectrometer (GF-AAS, Model: PerkinElmer). The amounts of As(V) or F^- anions adsorbed on the Al_2O_3/CSC were calculated from the difference between the initial concentration (C_0) and the equilibrium one (C_e). Adsorption performance was expressed in terms of adsorption percentage (%) and the distribution coefficient (K_d), which were calculated from the following equations:

$$\text{adsorption } \% = \frac{C_0 - C_e}{C_0} \times 100\% \quad (1)$$

$$K_d = \frac{C_0 - C_e}{C_e} \times \frac{V}{m} \quad (2)$$

where C_0 (mg/L) and C_e (mg/L) stand for the initial and equilibrium concentrations, respectively. V (mL) represents the suspension volume, and m (g) is the weight of adsorbent. All of the experimental data were the averages of triplicate determinations, and the relative errors of the data were less than 5%.

The stability and recycle property of the Al_2O_3/CSC were investigated by repeating the adsorption/desorption experiments for 6 cycles and the results were applied to evaluate the application performance of the Al_2O_3/CSC. NaOH was selected as the eluent to regenerate the Al_2O_3/CSC. Briefly, after the adsorption process, adsorbent was separated from suspension and added into 0.05 mol/L NaOH solution, shaken for 4 h. Then, adsorbent was separated and rinsed by Milli-Q water until no As(V) was detected in the rinsing solution. The Al_2O_3/CSC were dried in vacuum chamber and reused.

2.5. Natural Groundwater Sample. A natural groundwater sample was collected from Xing-Wang Village in Togtoh county, Inner Mongolia Autonomous Region, China (40.392924° N, 111.274188° E) (see the Supporting Information, Figure S2). One can see that the high As(V) area spread across the middle part and north part of China. Almost all of the northern China regions were As(V) contaminated, especially the Inner Mongolia Autonomous Region. The water sample was pumped out from a groundwater well, which was used as drinking water for local residents. The As(V) concentration of the water sample was analyzed by an atomic fluorescence spectrometry (AFS-230, Beijing Wantuo Instrument Co. Ltd., Beijing, China).

3. RESULTS AND DISCUSSION

3.1. Characterization. The microstructure and morphology of CSC, raw Al_2O_3 and $2Al_2O_3$/CSC were characterized by SEM and TEM images (Figure 2). As can be seen, the CSC sample possesses a hollow structure and numerous irregular holes with an average diameter of about 200 nm (Figure 2A). A magnified image (Figure 2B) demonstrates that the surface is uneven and the winkles may explain the large specific surface area of CSC. Figure 2C shows that the surface of CSC turns rough after combination with Al_2O_3 and the basic structure of CSC is maintained. The $2Al_2O_3$/CSC (Figure 2D) show that tiny needle-like Al_2O_3 is formed on the surface of CSC, making a rough CSC surface. The TEM images (Figure 2E and F)

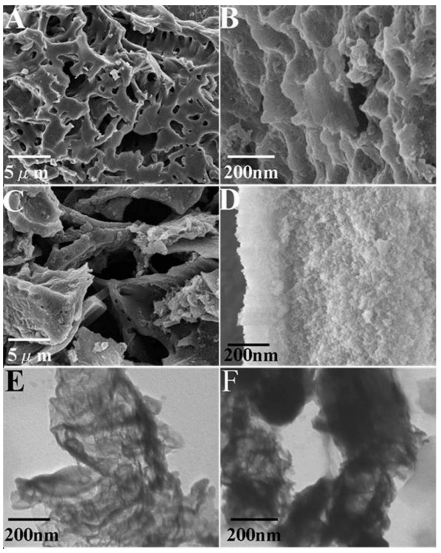

Figure 2. SEM images (A and B) and TEM image (E) of CSC. SEM images (C and D) and TEM image (F) of $2Al_2O_3$/CSC.

demonstrate a typical porous carbon structure and the layer of the sample turns thick after modification, indicating coverage of Al_2O_3 on the CSC surface.

The EDS analysis of the CSC in Figure 3A shows that carbon element possesses the dominating atomic ratio of 84.29% and the nitrogen and oxygen element have an atomic ratio of 7.33% and 1.31%, respectively. About 2% silica in the EDS spectrum is observed which could be attributed to the impurity in the CSC, and the 5% copper element in the EDS spectrum is attributed to the interference from the copper template.

The XRD patterns of Al_2O_3, CSC, and $2Al_2O_3$/CSC are presented in Figure 3B; the peaks at about 35°, 45°, and 67° in both Al_2O_3 and $2Al_2O_3$/CSC patterns confirm the preserve of γ-Al_2O_3 phases after integration, which is consistent with Pillewan's observation.[14] The weak peak of CSC at ~25° is attributed to the characteristic adsorption of C and the peak emerged in CSC pattern at 14.3° belongs to the impurity phase of boehmite.[23]

The BET analyses show that the specific surface areas of raw Al_2O_3 and CSC (Figure. 3C) are 45.73 and 214.94 m^2/g, respectively. The $2Al_2O_3$/CSC possesses a specific surface area of 90.70 m^2/g (Figure. 3C). It is apparent that the BET specific surface area of $2Al_2O_3$/CSC is much higher than that of raw Al_2O_3.

To achieve a better understanding of the adsorption mechanism, CSC, nitric acid-treated CSC, raw Al_2O_3, and $2Al_2O_3$/CSC samples before/after As(V) adsorption were characterized by FT-IR. In Figure 3D, CSC shows no obvious adsorption peaks, indicating a pure carbon sample with no functional groups was obtained. However, obvious peaks at 3458, 2918, 2850, and 1710 cm^{-1} could be observed in the spectrum of nitric acid-treated CSC, which correspond to O−H vibration, sp^2 carbon, sp^3 carbon, and C═O vibration, respectively. The similar phenomenon was also observed in Mahanta's study,[17] which reveals the formation of −OH and −COOH on the surface of CSC. For the FT-IR spectra of Al_2O_3, $2Al_2O_3$/CSC, and As(V) adsorbed $2Al_2O_3$/CSC, the broad peak at 3458 cm^{-1} and the sharp peak at 1634 cm^{-1} could be attributed to O−H vibration and H−O−H bending, respectively.[21] After As(V) adsorption, the peak at 3458 cm^{-1} becomes weak and a new As−O vibration peak at ~1120 cm^{-1}

dx.doi.org/10.1021/ie503057g | Ind. Eng. Chem. Res. 2014, 53, 16051−16060

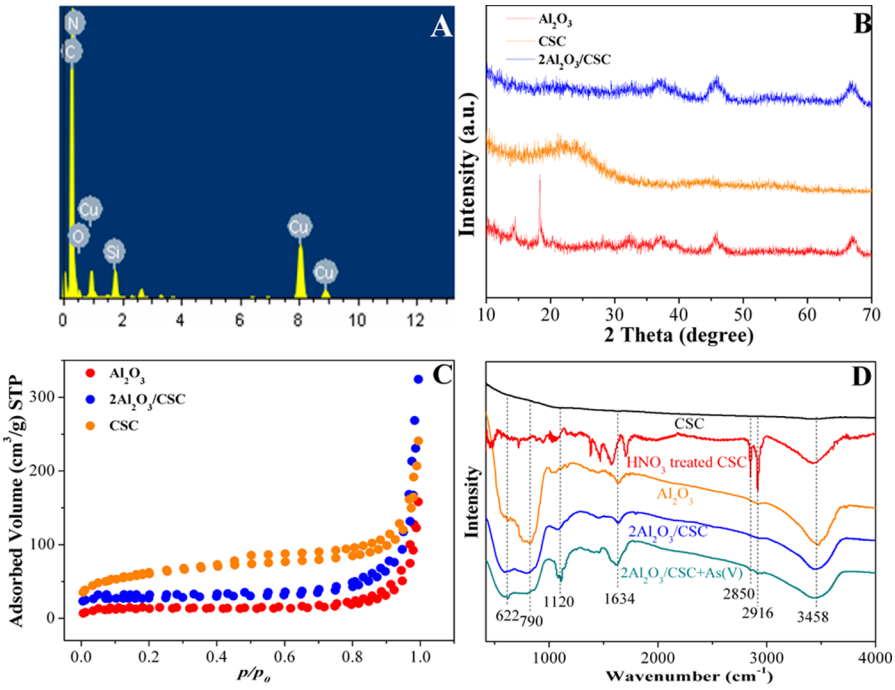

Figure 3. EDS analysis of CSC (A); XRD patterns of CSC, raw Al_2O_3 and $2Al_2O_3$/CSC (B); N_2 adsorption−desorption isotherms for raw Al_2O_3, CSC, and $2Al_2O_3$/CSC (C); FT-IR spectra of cigarette soot carbon, raw Al_2O_3, $2Al_2O_3$/CSC, and As(V) adsorbed $2Al_2O_3$/CSC (D).

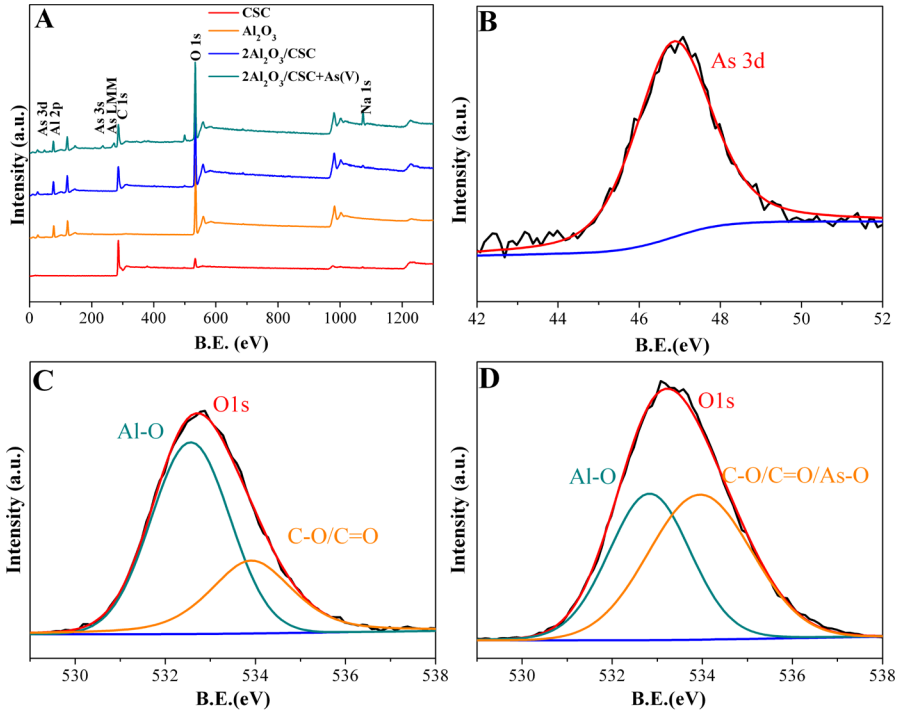

Figure 4. XPS spectra of $2Al_2O_3$/CSC and As(V) adsorbed $2Al_2O_3$/CSC (A); high resolution XPS spectra of As 3d spectrum of As(V) adsorbed $2Al_2O_3$/CSC (B); high resolution XPS O 1s core-level spectrum of $2Al_2O_3$/CSC (C) and As(V) adsorbed $2Al_2O_3$/CSC (D).

is observed, suggesting the presence of adsorbed As(V) on the solid surfaces. The small peak of Si−O vibration at 1076 cm^{-1} can be attributed to the trace amount of Si in CSC.[24] The peaks at ~790 and ~622 cm^{-1} are the typical Al−O lattice vibrations,[25] of which the peak at 622 cm^{-1} becomes stronger while the peak at 790 cm^{-1} almost vanishes after As(V) adsorption. This observation indicates the breaking of Al−OH bond and the new formation of Al−O−As bond. Therefore, a reasonable interpretation of the adsorption mechanism is the interactions between negative charged As(V) anions and positive charged Al_2O_3 surface.

The XPS technique was further applied to test the surface state of $2Al_2O_3$/CSC and the As(V) adsorbed $2Al_2O_3$/CSC (Figure 4). In Figure 4A, the strong C 1s peak in CSC spectrum indicates carbon is the main element and the weak O 1s peak may be attributed to −OH and −COOH groups. In the

dx.doi.org/10.1021/ie503057g | Ind. Eng. Chem. Res. 2014, 53, 16051−16060

spectrum of raw Al_2O_3, the stronger O 1s peak reveals that more oxygen is contained as comparing with CSC. The strong peaks of O 1s, C 1s, and Al 2p show that oxygen, aluminum, and carbon are the predominant elements of the samples (before and after As(V) adsorption). A noticeable Na 1s peak could be observed on the As(V) adsorbed $2Al_2O_3$/CSC spectrum, which is attributed to the added NaCl in suspension. A series of As peaks including: As 3d, As 3s, and As LMM could be observed in the As(V) adsorbed $2Al_2O_3$/CSC spectrum, which suggests the adsorption of As(V) on $2Al_2O_3$/CSC surface. Figure 4B exhibits a high resolution XPS spectrum of As(V) adsorbed $2Al_2O_3$/CSC. The clear As 3d peak at the binding energy of 46.7 eV confirms the presence of arsenic species on the surface of adsorbent, which is similar to the previous report.[17] The high resolution O 1s XPS spectra of the $2Al_2O_3$/CSC before and after As(V) adsorption are shown in Figure 4C and D. The strong peak at binding energy of 532.5 eV at Figure 4C can be assigned to Al−O adsorption and the weak peak at 533.9 eV could be attributed to the C−O or C═O on adsorbent surface. In Figure 4D, it can be seen that the peak intensity of Al−O at 532.5 eV decreases dramatically while the peak at 533.9 eV increases after the As(V) adsorption. After the interaction with $2Al_2O_3$/CSC, the combined intensity of C−O/C═O/As−O increases obviously as comparing to the peak before As(V) adsorption. Besides, the peak intensity of O 1s turns stronger after As(V) adsorption, which could be assigned to various bonded oxygen between adsorbent and arsenate species.[17] This phenomenon may be an evidence of the formation of Al−O−As bond.

3.2. Time Dependent Adsorption. Adsorption kinetics represents the uptake rate and reflects adsorption efficiency. The adsorption of As(V) on the synthesized $2Al_2O_3$/CSC are investigated at pH 5.5 ± 0.1 at an adsorbent content of 0.2 g/L. As a comparison, the adsorption kinetics of As(V) adsorption on raw Al_2O_3 are also conducted. To investigate the adsorption kinetics, the As(V) adsorption curves are simulated by pseudo-first-order and pseudo-second-order models, respectively, and the simulation equations are presented as follows:[26]

$$\log(q_e - q_t) = \log q_e - \frac{k_1}{2.303}t \quad (3)$$

$$\frac{t}{q_t} = \frac{1}{k_2 q_e^{\,2}} + \frac{t}{q_e} \quad (4)$$

where q_e (mg/g) and q_t (mg/g) represent the amounts of As(V) adsorbed at equilibrium and at contact time t (h), respectively. Here k_1 (h^{-1}) is the pseudo-first-order rate constant, and k_2 (g/mg/h) is the pseudo-second-order rate constant. The values of k_1 and q_e in the pseudo-first-order equation are obtained from the slope and intercept by plotting $\log(q_e - q_t)$ versus t, whereas, k_2 and q_e in the pseudo-second-order equation are obtained by plotting t/q_t vs t.

Figure 5 shows the simulation results of As(V) adsorption kinetics, the As(V) absorption percentage on $2Al_2O_3$/CSC increase considerably fast in the first contact time of 2.0 h, and then keeps stable at ∼75% from 2.0 to 12.0 h. By comparison, the As(V) adsorption on raw Al_2O_3 is completed within 3.0 h of contact time and ∼52% As(V) is removed at the adsorption equilibrium. The As(V) adsorption on pure CSC was also performed, the adsorption achieves equilibrium at 1.5 h of contacting time with a removal percentage of 15.7%. The rapid As(V) adsorption rate indicates that the adsorption mechanism is mainly attributed to chemical interaction or inner-sphere

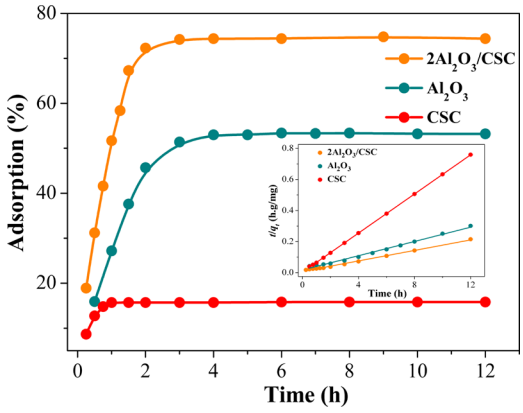

Figure 5. Adsorption kinetics of As(V) on $2Al_2O_3$/CSC, raw Al_2O_3, and CSC (T = 293 K, m/V = 0.2 g/L, $C_{[As(V)]initial}$ = 0.5 mmol/L (37.5 mg/L), I = 0.01 mol/L NaCl, pH = 5.5 ± 0.1), as well as the inserted linear plots of pseudo-second-order kinetic for As(V) adsorption on $2Al_2O_3$/CSC and on raw Al_2O_3.

surface complexation.[27] The linear plots of pseudo-second-order kinetic for As(V) adsorption on $2Al_2O_3$/CSC and on raw Al_2O_3 are inserted in Figure 5 and the relative parameters calculated are listed in Table S1. Apparently, the correlation coefficient of pseudo-second-order model is much closer to 1.0 than that of pseudo-first-order model, suggesting a chemisorption process.[22]

3.3. Effect of Solution pH. The removal of As(V) is highly pH-dependent due to the changes of solution pH could impact the relative distribution of As(V) species and the surface charges of the adsorbents, resulting in either promoting or suppressing As(V) adsorption on adsorbent surface. Experiments of pH impaction are conducted to calculate the efficiency of $2Al_2O_3$/CSC at different pH values. For comparison purpose, tests of pH effect toward As(V) adsorption on raw Al_2O_3 are also performed, and the results are shown in Figure 6A. It can be seen that the $2Al_2O_3$/CSC exhibits a higher adsorption capacity to As(V) than pure Al_2O_3 at the same experimental conditions. The As(V) adsorption reaches the highest adsorption percentage at pH ∼ 5.0, where ∼80% As(V) is adsorbed on the synthesized $2Al_2O_3$/CSC, and then decreases significantly from ∼80% to ∼10% as the solution pH increases from 5.0 to 11.0. The stability of $2Al_2O_3$/CSC at different pH values was also investigated by mixing certain amount of adsorbent in different pH solutions for 3 h. Then it was separated, dried and weighted. As shown in Figure 6B, no decrease of the adsorbent weight emerged at pH 5.0 and 6.0, a slight amount of $2Al_2O_3$/CSC was dissolved at pH 4.0 and about 93% of the $2Al_2O_3$/CSC was retrieved after processing in pH 3.0 solution.

To further investigate the influence of pH on As(V) uptake, the surface properties of raw Al_2O_3 and $2Al_2O_3$/CSC in aqueous solution are analyzed by acid−base surface titrations (Figure 6C). The point of zero charge (pH_{pzc}) at which the surface charge becomes neutral, is calculated by plotting the total concentration of consumed protons (TOTH) to the suspension pH. The pH_{pzc} values of Al_2O_3 and $2Al_2O_3$/CSC are estimated to be 7.20 and 7.88, respectively, which is consistent with the previous report.[19]

The pH_{pzc} is an intrinsic property of the interface between solid and liquid which is mainly determined by crystallinity of the solid and chemical nature. The $2Al_2O_3$/CSC is positively

dx.doi.org/10.1021/ie503057g | Ind. Eng. Chem. Res. 2014, 53, 16051−16060

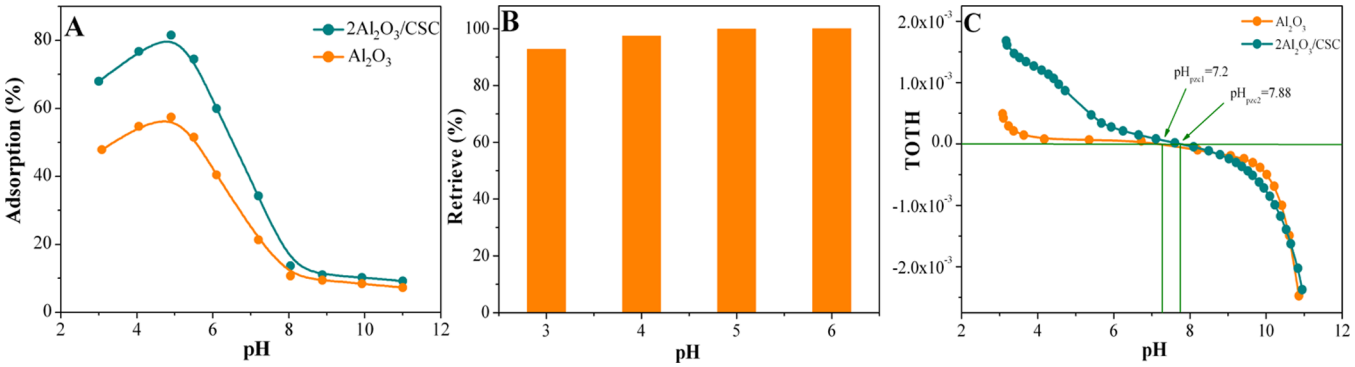

Figure 6. Effect of pH on As(V) adsorption onto raw Al_2O_3 and $2Al_2O_3$/CSC (T = 293 K, m/V = 0.2 g/L, $C_{[As(V)]initial}$= 0.5 mmol/L (37.5 mg/L), I = 0.01 mol/L NaCl) (A); stability of $2Al_2O_3$/CSC at different pH values (T = 293 K, m/V = 0.2 g/L) (B); TOTH of raw Al_2O_3 and $2Al_2O_3$/CSC as a function of pH (T = 293 K, m/V = 0.2 g/L, I = 0.01 mol/L NaCl) (C).

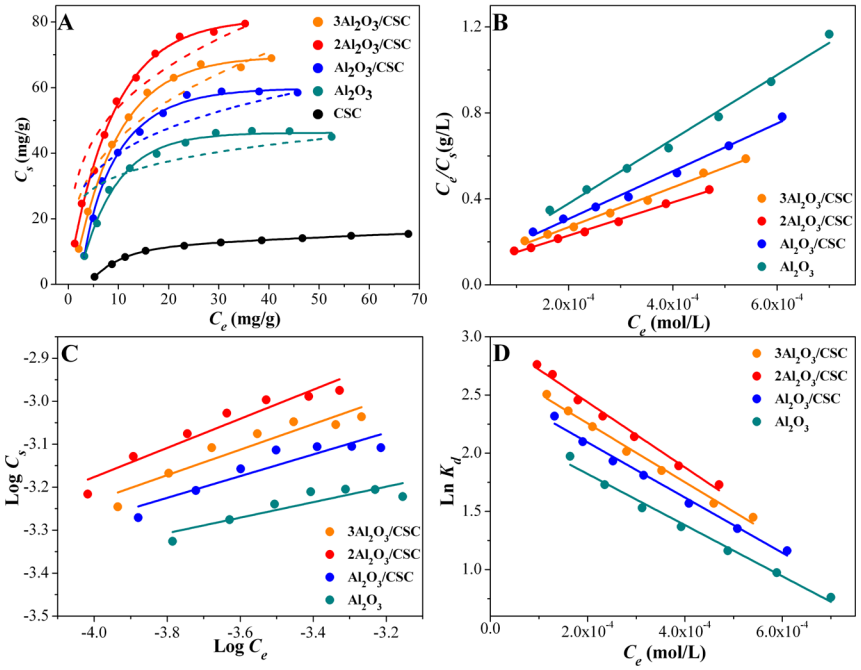

Figure 7. Adsorption isotherms of As(V) on CSC, raw Al_2O_3, Al_2O_3/CSC, $2Al_2O_3$/CSC, and $3Al_2O_3$/CSC (A); linear plots of Langmuir model of the As(V) adsorption on raw Al_2O_3, Al_2O_3/CSC, $2Al_2O_3$/CSC, and $3Al_2O_3$/CSC (B); linear plots of Freundlich model of the As(V) adsorption on raw Al_2O_3, Al_2O_3/CSC, $2Al_2O_3$/CSC, and $3Al_2O_3$/CSC (C); linear plots of ln K_d versus C_e (D): m/V = 0.2 g/L, T = 293 K, $C_{[As(V)]initial}$ = 0.5 mmol/L, pH = 5.5 ± 0.1, I = 0.01 mol/L NaCl.

charged in the pH range of 3.0−7.88 via the protonation reaction:

$$\equiv Al—OH \xrightarrow{+H^+} \equiv Al—OH_2^-$$

and then becomes negatively charged in the pH range of 7.88−11.0 through the deprotonation reaction:

$$\equiv Al—OH \xrightarrow{-H^+} \equiv Al—OH^-$$

due to the presence of OH^- in solution. As a typical amphoteric metal oxide, Al_2O_3 is soluble in strong acidic or alkaline solutions but insoluble in neutral solutions, which could be presented as

$$\equiv Al—OH_2^+ \xleftarrow{+H^+} \underset{pH_{pzc}}{\equiv Al—OH} \xrightarrow{-H^+} \equiv Al—OH^-$$

The titration curve of $2Al_2O_3$/CSC locates on the upside of the Al_2O_3 curve at pH < pH_{pzc}, suggesting that the $2Al_2O_3$/CSC possess a more positive surface. The highly efficient As(V) adsorption at low pH values is attributed to the positive charges of $2Al_2O_3$/CSC surface. Whereas at pH > pH_{pzc}, the surfaces are negatively charged and the As(V) anions adsorption is suppressed due to the electrostatic repulsion. As(V) presents different species at different pH values (see the Supporting Information, Figure S3). The dominate species is $H_2AsO_4^-$ within the pH range of 3.0−6.8, which is more favorable to be adsorbed on $2Al_2O_3$/CSC surface.[28] In this part, the adsorption can be described as $Al(OH)_2^+ + H_2AsO_4^- \rightarrow Al(OH)_2—H_2AsO_4$. At pH 6.8−11.5, the As(V) anion carries 2 negative charges and presents in the form of $HAsO_4^{2-}$, the adsorption can be described as $2Al(OH)_2^+ + HAsO_4^{2-} \rightarrow H_2AsO_4—Al(OH)_2—H_2AsO_4$. In this part, the As(V) adsorption percentage is reduced due to the exclusion between $HAsO_4^{2-}$ and the negatively charged adsorbent surface.[29] In high pH section (pH > 11.5), a part of Al_2O_3 on $2Al_2O_3$/CSC surface is gradually dissolved and the As(V) adsorption is not discussed

dx.doi.org/10.1021/ie503057g | Ind. Eng. Chem. Res. 2014, 53, 16051−16060

here. Herein, the impact of pH toward As(V) adsorption on the synthesized $2Al_2O_3$/CSC may be partly attributed to electrostatic interactions.

3.4. Adsorption Isotherms and Mechanism. To explore the best adsorption performance to As(V) by the synthesized adsorbents, the As(V) adsorption isotherms on series of Al_2O_3/CSC and pure CSC at 293 K are shown in Figure 7A. It is obvious that the adsorption capacity of CSC (11.7 mg/g) is quite low compared to that of Al_2O_3/CSC materials (96.9 mg/g) at the same condition. To achieve a better understanding of the adsorption thermodynamics, the adsorption isotherms at 303 and 313 K are also studied (see Supporting Information Figure S4 and S5, respectively). It is apparent that all the isotherms show an increasing tendency and the adsorption increment gradually slow down as As(V) concentration increases. For adsorption modeling purposes, Langmuir and Freundlich models are applied to describe the As(V) adsorption on Al_2O_3/CSC, respectively. The Langmuir isotherm model was used to describe monolayer adsorption on the basis of following assumptions, i.e., the surface with homogeneous binding sites, equivalent adsorption energies, and no interaction between adsorbed species. It can be expressed as follows:[30]

$$C_s = \frac{bC_{smax}C_e}{1 + bC_e} \tag{5}$$

The equation can be modified to linear form:

$$\frac{C_e}{C_s} = \frac{1}{bC_{smax}} + \frac{C_e}{C_{smax}} \tag{6}$$

where C_e (mol/L) and C_{smax} (mol/g) are the equilibrium concentration of As(V) in solution and the maximum As(V) adsorption capacity on the adsorbent, respectively. The term b (L/mol) is a Langmuir constant that relates to energy of adsorption.

The Freundlich isotherm model is applicable for several types of adsorption sites on the adsorbent surface and it is in accordance with the adsorption data at low and intermediate concentrations on heterogeneous surfaces. The model can be expressed by the following equation:[31]

$$C_s = K_F C_e^{\,n} \tag{7}$$

The equation can be expressed in linear form:

$$\log C_s = \log K_F + n \log C_e \tag{8}$$

where K_F ($mol^{1-n}\cdot L^n/g$) and n are Freundlich constants representing the adsorption capacity when As(V) anions equilibrium concentration equals 1 and adsorption intensity, respectively.

Simulation curves at 293 K are shown in Figure 7A, the solid lines and dash lines represent Langmuir model and Freundlich model, respectively. Accordingly, fitting parameters at 293 K, obtained from the linear plots (Figure 7B and C), are listed in Table S2. The fitting curves displayed in Figure 7A and correlation coefficients (R^2) listed in Table S2 suggest a better description of Langmuir model than Freundlich model. The series of Al_2O_3/CSC with varying Al_2O_3 amount show an enhanced As(V) removal capability than pure Al_2O_3 due to the porous structure of CSC. For comparison, the maximum adsorption capacities (C_{smax}) of As(V) on different adsorbents reported in previous literatures are collected and tabulated in Table S3. The highest As(V) adsorption performance of 96.9 mg/g was achieved on $2Al_2O_3$/CSC as compared with previous reported adsorbents such as hematite (0.2 mg/g),[32] Goethite (5 mg/g),[33] GAC-FeNaClO (0.05 M) (6.57 mg/g),[34] Fe10SBA-15 (12.74 mg/g),[35] ferrihydrite (68.75 mg/g),[36] zirconium-(IV)-loaded phosphoric chelate adsorbent (149.9 mg/g),[37] and Fe(III) alginate gel (352 mg/g).[38] High As(V) removal performance could be achieved by the chelation between As(V) and the functional groups of adsorbents.[37,38] In this case, the BET surface area of Al_2O_3 is greatly enlarged after the modification with CSC. As a surface reaction, the As(V) adsorption is accomplished via the interaction between As(V) anions and the positive charged Al_2O_3 surface, which will be enhanced with the increment of the interface between As(V) solution and $2Al_2O_3$/CSC. With the promoting of interface between adsorbent and adsorbate, more binding sites will be available and more As(V) are interacted with the binding sites during the adsorption process, that is, more As(V) are removed. Besides, good dispersion in aqueous solutions can also improve the adsorption. Therefore, the marvelous adsorption capacity of $2Al_2O_3$/CSC to As(V) anions may be attributed to the porous structure and the large contacting interface between As(V) and $2Al_2O_3$/CSC in solutions.

Thermodynamic parameters (i.e., ΔG^0, ΔS^0, and ΔH^0) of As(V) adsorption on the synthesized adsorbents calculated from the temperature-dependent isotherms were used to investigate the interaction mechanism. The value of Gibbs free energy change (ΔG^0) could be obtained from the function:[39]

$$\Delta G^\circ = -RT \ln K^0 \tag{9}$$

where R is the ideal gas constant (8.3145 J/mol/K) and T (K) is the Kelvin temperature. K^0 is the thermodynamic equilibrium constant, the values of $\ln K^0$ are obtained by plotting $\ln K_d$ as a function of C_e and extrapolating C_e to zero. Linear fits of the equation at 293 K are shown in Figure 7D. The average standard enthalpy change (ΔH^0) could be obtained from the van't Hoff equation:[39]

$$\ln K^0(T_2) - \ln K^0(T_1) = \frac{-\Delta H^0}{R}\left(\frac{1}{T_2} - \frac{1}{T_1}\right) \tag{10}$$

where T_2 and T_1 are two different temperatures. The standard entropy change (ΔS^0) could be calculated from the relationship:[39]

$$\Delta S^\circ = -\frac{\Delta G^\circ - \Delta H^\circ}{T} \tag{11}$$

The thermodynamic parameters are tabulated in Table S4. The negative ΔG^0 values reveal that the As(V) adsorption on the synthesized adsorbents are spontaneous processes and the minimum ΔG^0 values (−5.07, −5.48, −5.78 kJ/mol at 293, 303, 313 K, respectively) are obtained on $2Al_2O_3$/CSC, indicating that $2Al_2O_3$/CSC possess the strongest reacting tendency. The positive ΔH^0 values of As(V) adsorption on the synthesized $2Al_2O_3$/CSC indicate that the adsorption is endothermic, and it is in accordance with the fact that the adsorption is facilitated at high temperature.[26] The positive values of the entropy change (ΔS^0) may be attributed to the change of As(V) species and the formation of As−O−Al bond. Thermodynamic parameters show that the As(V) adsorption on the synthesized adsorbents is an endothermic process and could be accomplished spontaneously.

dx.doi.org/10.1021/ie503057g | Ind. Eng. Chem. Res. 2014, 53, 16051−16060

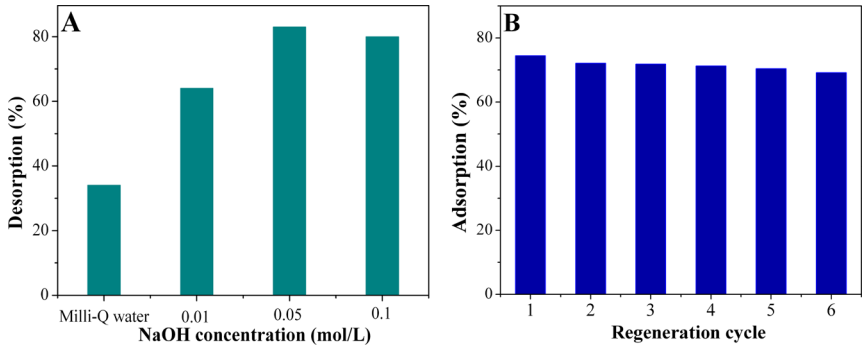

Figure 8. Effect of alkaline concentration on As(V) desorption from $2Al_2O_3$/CSC (m/V = 0.2 g/L, T = 293 K, I = 0.01 mol/L NaCl) (A); regeneration tests of As(V) adsorption on $2Al_2O_3$/CSC (m/V = 0.2 g/L, T = 293 K, $C_{[As(V)]initial}$ = 0.5 mmol/L, pH = 5.5 ± 0.1, I = 0.01 mol/L NaCl) (B).

3.5. Regeneration Experiments. In Figure 6A, the As(V) adsorption is low in high pH solutions, suggesting that the As(V) adsorption on $2Al_2O_3$/CSC could be desorbed by alkaline solution. Therefore, desorption experiments are conducted in sodium hydroxide solutions (0.01−0.1 mol/L) and Milli-Q water is used for comparison. To avoid the dissolution of adsorbent, desorption tests are completed within 1 h.[19] The desorption percentages are 64%, 83%, 80%, and 31% in 0.01, 0.05, 0.1 mol/L NaOH and Milli-Q water (Figure 8A), respectively. From Figure 6A, one can see that the adsorption of As(V) on the $2Al_2O_3$/CSC decreases obviously with increasing pH in the pH range of 5−8 and then decreases slowly with increasing pH at pH > 8. Herein, the differences in the desorption of As(V) in 0.05 and 0.1 mol/L NaOH solutions may be attributed to the relative data errors. Milli-Q water shows a slight desorption percentage due to the new equilibrium achieved between As(V) and $2Al_2O_3$/CSC in solution.

Six cycles of adsorption/desorption tests are conducted to evaluate the long-term performance of this material in practical wastewater treatment. As can be seen from Figure 8B, the adsorption capacity of $2Al_2O_3$/CSC toward As(V) decreases slightly from 75% to 69% after six rounds. In desorption tests, the desorbed $2Al_2O_3$/CSC were separated, dried and weighted; about 87% of the adsorbent was retrieved at last. The feasible adsorption/desorption property suggests that the $2Al_2O_3$/CSC could be used for many times for the elimination of As(V) from aqueous solutions in actual applications.

3.6. Natural Groundwater Treatment. The elimination of As(V) from actual groundwater by using $2Al_2O_3$/CSC was investigated to evaluate the application of $2Al_2O_3$/CSC in actual applications. The As(V) concentration in the natural groundwater sample is determined to be 233 μg/L, and a fluoride (F^-) concentration of 4.14 mg/L is also detected. An electrochemical method by using expandable ion analyzer with F^- ion selective electrode PF-202-CF (Leici, China) was applied to analyze F^- concentrations in groundwater sample.[40] The main components of the groundwater are listed in Table S5. As a main water pollutant, anionic F^- ions could be adsorbed on the positive charged adsorbent surface, which is also investigated in the batch experiments, the adsorption isotherm (Figure S6) suggests $2Al_2O_3$/CSC possess a maximum adsorption capacity of 101.7 mg/g to F^-. According to experimental results, the $2Al_2O_3$/CSC show the best adsorption capacity to As(V) which is also selected for the depuration of actual groundwater sample. The original pH of the actual groundwater sample is detected to be 8.37 and the groundwater sample is used directly without any further treatment in the experiment process. Briefly, 0.2 g of $2Al_2O_3$/CSC is dispersed in 20 mL actual groundwater sample in a 25 mL glass vial. The suspensions are shaken for 24 h and then keeps static for 4 h. Results show that more than 96% As(V) and about 98% F^- are removed from the initial groundwater sample with the final concentrations of As(V) and F^- to be 8 μg/L and 0.083 mg/L, respectively. Both concentrations are lower than the current WHO requirements of 10 μg/L for As(V) and 1.5 mg/L for F^-.[6] To further investigate the removal performance, an experiment of adsorbent concentration effect is conducted. As shown in Figure 9, to achieve the WHO

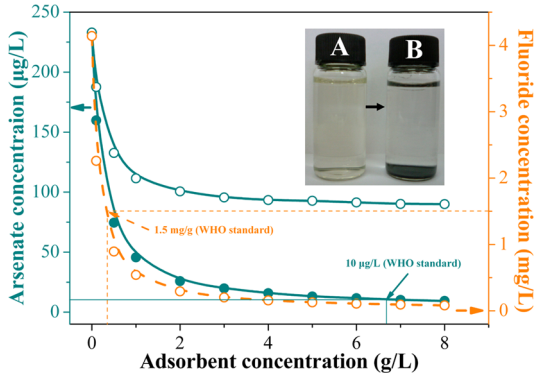

Figure 9. Effect of adsorbent content on As(V) and F^- removal from natural groundwater sample. The dark blue−green line is for As(V) removal (open circle for CSC and full circle for $2Al_2O_3$/CSC), and the orange line is for F^- removal by $2Al_2O_3$/CSC, T = 293 K, $C_{[As(V)]initial}$ = 233 μg/L, $C_{[F^-]initial}$ = 4.14 mg/g.

drinking water standard, a minimum $2Al_2O_3$/CSC content of 7 g/L is required to remove As(V) and F^- from the actual groundwater. By comparison, the removal curve of As(V) on CSC indicates the purified water can not reach the WHO standard if only treated with CSC. An image of actual groundwater sample before and after adsorption is inserted in Figure 9; image A is the natural groundwater sample, and image B reveals that the $2Al_2O_3$/CSC are subsided to the vial bottom and the supernatant is much clearer than the initial one. The results indicate that the as-synthesized $2Al_2O_3$/CSC may possess potential applications in the purification of contaminated drinking water in actual water pollution cleanup.

dx.doi.org/10.1021/ie503057g | Ind. Eng. Chem. Res. 2014, 53, 16051−16060

4. CONCLUSIONS

In this work, Al_2O_3 is modified by CSC with varying Al_2O_3/CSC ratios to fabricated Al_2O_3/CSC by thermal method. The maximum adsorption capacity, achieved by $2Al_2O_3$/CSC, reaches 96.9 mg/g at pH 5.5. Results show that As(V) adsorption on Al_2O_3/CSC is accomplished by forming outer-sphere surface complexes. The adsorption isotherms fit the Langmuir model well, which suggests that the As(V) removal is a monolayer process. A regeneration test shows that the $2Al_2O_3$/CSC could be used at least 6 times (or even more times) without significant decrement of adsorption capacity. More than 96% As(V) and 98% F^- ions are removed from both As(V) rich and F^- rich natural groundwater sample obtained in Inner Mongolia county. Therefore, $2Al_2O_3$/CSC could be a favorable low-priced adsorbent for the depuration of both As(V) and F^- contaminated groundwater.

■ ASSOCIATED CONTENT

Supporting Information

Sample image of CSC (Figure S1), As(V) distribution of China (Figure S2), As(V) species distribution (Figure S3), isotherms at 303 (Figure S4) and 313 K (Figure S5), F^- adsorption isotherm (Figure S6), parameters of kinetics study (Table S1), parameters for As(V) adsorption isotherms simulation (Table S2), comparison of maximum As(V) adsorption capacity among different adsorbents (Table S3), parameters of As(V) adsorption thermodynamic study (Table S4), and component of groundwater sample (Table S5). This material is available free of charge via the Internet at http://pubs.acs.org/.

■ AUTHOR INFORMATION

Corresponding Author

*Fax: +86-551-65591310. Phone: +86-551-65593308. E-mail: lijx@ipp.ac.cn.

Notes

The authors declare no competing financial interest.

■ ACKNOWLEDGMENTS

Financial support from the National Natural Science Foundation of China (21207136, 21225730, 91326202, and 21207135), 973 project (2011CB933700), and Hefei Center for Physical Science and Technology (2012FXZY005) are acknowledged. The great assistance for fluoride analysis from Nantong Zhang, Hefei Institute of Intelligent Machines, Chinese Academy of Sciences, is also acknowledged.

■ REFERENCES

(1) Mandal, B. K.; Suzuki, K. T. As(V) round the world: a review. *Talanta* **2002**, *58*, 201.

(2) Smedley, P. L.; Kinniburgh, D. G.; Macdonald, D. M. J.; Nicolli, H. B.; Barros, A. J.; Tullio, J. O.; Pearce, J. M.; Alonso, M. S. As(V) associations in sediments from the loess aquifer of La Pampa, Argentina. *Appl. Geochem.* **2005**, *20*, 989.

(3) Mohan, D.; Pittman, C. U. As(V) removal from water/wastewater using adsorbents - A critical review. *J. Hazard. Mater.* **2007**, *142*, 1.

(4) Smedley, P. L.; Kinniburgh, D. G. A review of the source, behaviour and distribution of As(V) in natural waters. *Appl. Geochem.* **2002**, *17*, 517.

(5) Mertens, J.; Rose, J.; Kagi, R.; Chaurand, P.; Plotze, M.; Wehrli, B.; Furrer, G. Adsorption of As(V) on polyaluminum granulate. *Environ. Sci. Technol.* **2012**, *46*, 7310.

(6) World Health Organization. *Guidelines for Drinking Water Quality*, 1; Geneva, 1993.

(7) Sabbatini, P.; Yrazu, F.; Rossi, F.; Thern, G.; Marajofsky, A.; de Cortalezzi, M. M. F. Fabrication and characterization of iron oxide ceramic membranes for As(V) removal. *Water Res.* **2010**, *44*, 5702.

(8) Ghosh, R. K.; Reddy, D. D. Tobacco Stem Ash as an Adsorbent for Removal of Methylene Blue from Aqueous Solution: Equilibrium, Kinetics, and Mechanism of Adsorption. *Water Air Soil Poll.* **2013**, *224*, 1582.

(9) Annadurai, G.; Juang, R. S.; Lee, D. J. Use of cellulose-based wastes for adsorption of dyes from aqueous solutions. *J. Hazard. Mater.* **2002**, *92*, 263.

(10) Tsai, W. T.; Hsu, H. C.; Su, T. Y.; Lin, K. Y.; Lin, C. M. Removal of basic dye (methylene blue) from wastewaters utilizing beer brewery waste. *J. Hazard. Mater.* **2008**, *154*, 73.

(11) Chen, X. G.; Lv, S. S.; Liu, S. T.; Zhang, P. P.; Zhang, A. B.; Sun, J.; Ye, Y. Adsorption of Methylene Blue by Rice Hull Ash. *Sep. Sci. Technol.* **2012**, *47*, 147.

(12) Wang, S. B.; Zhu, Z. H. Sonochemical treatment of fly ash for dye removal from wastewater. *J. Hazard. Mater.* **2005**, *126*, 91.

(13) Zhang, S. W.; Zeng, M. Y.; Li, J. X.; Xu, J. Z.; Wang, X. K. Porous magnetic carbon sheets from biomass as an adsorbent for the fast removal of organic pollutants from aqueous solution. *J. Mater. Chem. A* **2014**, *2*, 4391.

(14) Pillewan, P.; Mukherjee, S.; Roychowdhury, T.; Das, S.; Bansiwal, A.; Rayalu, S. Removal of As(III) and As(V) from water by copper oxide incorporated mesoporous alumina. *J.Hazard. Mater.* **2011**, *186*, 367.

(15) Zhang, W.; Fu, J.; Zhang, G.; Zhang, X. Enhanced arsenate removal by novel Fe-La composite (hydr)oxides synthesized via coprecipitation. *Chem. Eng. J.* **2014**, *251*, 69.

(16) Guo, Q.; Tian, J. Removal of fluoride and arsenate from aqueous solution by hydrocalumite via precipitation and anion exchange. *Chem. Eng. J.* **2013**, *231*, 121.

(17) Mahanta, N.; Chen, J. P. Document a novel route to the engineering of zirconium immobilized nano-scale carbon for arsenate removal from water. *J. Mater. Chem. A* **2013**, *1*, 8636.

(18) Mohan, D.; Pittman, C. U. As(V) removal from water/wastewater using adsorbents - A critical review. *J. Hazard. Mater.* **2007**, *142*, 1.

(19) Kim, Y. H.; Kim, C. M.; Choi, I. H.; Rengaraj, S.; Yi, J. H. As(V) removal using mesoporous alumina prepared via a templating method. *Environ. Sci. Technol.* **2004**, *38*, 924.

(20) Zhang, M.; Gao, B. Removal of As(V), methylene blue, and phosphate by biochar/AlOOH nanocomposite. *Chem. Eng. J.* **2013**, *226*, 286.

(21) Wu, X. L.; Tan, X. L.; Yang, S. T.; Wen, T.; Guo, H. L.; Wang, X. K.; Xu, A. W. Coexistence of adsorption and coagulation processes of both arsenate and NOM from contaminated groundwater by nanocrystallined Mg/Al layered double hydroxides. *Water Res.* **2013**, *47*, 4159.

(22) Wen, T.; Wu, X. L.; Tan, X. L.; Wang, X. K.; Xu, A. W. One-pot synthesis of water-swellable Mg-Al layered double hydroxides and graphene oxide nanocomposites for efficient removal of As(V) from aqueous solutions. *ACS. Appl. Mater. Inter.* **2013**, *5*, 3304.

(23) Wang, Q.; Tay, H. H.; Guo, Z. H.; Chen, L. W.; Liu, Y.; Chang, J.; Zhong, Z. Y.; Luo, J. Z.; Borgna, A. Morphology and composition controllable synthesis of Mg-Al-CO_3 hydrotalcites by tuning the synthesis pH and the CO_2 capture capacity. *Appl. Clay. Sci.* **2012**, *55*, 18.

(24) Castaldi, P.; Silvetti, M.; Enzo, S.; Melis, P. Study of sorption processes and FT-IR analysis of arsenate sorbed onto red muds (a bauxite ore processing waste). *J. Hazard. Mater.* **2010**, *175*, 172.

(25) Wu, X. L.; Wang, L.; Chen, C. L.; Xu, A. W.; Wang, X. K. Water-dispersible magnetite-graphene-LDH composites for efficient arsenate removal. *J. Mater. Chem.* **2011**, *21*, 17353.

(26) Liu, M. C.; Chen, C. L.; Hu, J.; Wu, X. L.; Wang, X. K. Synthesis of Magnetite/Graphene Oxide Composite and Application for Cobalt(II) Removal. *J. Phys. Chem. C* **2011**, *115*, 25234.

(27) Yang, S. T.; Sheng, G. D.; Tan, X. L.; Hu, J.; Du, J. Z.; Montavon, G.; Wang, X. K. Determination of Ni(II) uptake mechanisms on mordenite surfaces: A combined macroscopic and microscopic approach. *Geochim. Cosmochim. Acta* **2011**, *75*, 6520.
(28) Xu, H.; Allard, B.; Grimvall, A. Effects of Acidification and Natural Organic Materials on the Mobility of As(V) in the Environment. *Water Air Soil Poll.* **1991**, *57−8*, 269.
(29) Bowers, A. R.; Huang, C. P. Adsorption Characteristics of Polyacetic Amino-Acids onto Hydrous Gamma-Al_2O_3. *J. Colloid Interface Sci.* **1985**, *105*, 197.
(30) Langmuir, I. The Adsorption of Gases on Plane Surfaces of Glass, Mica and Platinum. *J. Am. Chem. Soc.* **1918**, *40*, 1361.
(31) Walker, E. A.; Morton, P. Application of Freundlich Isotherm to Adsorption of Sugars from Solution by Column of Charcoal. *Analyst.* **1964**, *89*, 512.
(32) Singh, D. B.; Prasad, G.; Rupainwar, D. C. Adsorption technique for the treatment of As(V)-rich effluents. *Colloid Surface A* **1996**, *111*, 49.
(33) Lakshmipathiraj, P.; Narasimhan, B. R. V.; Prabhakar, S.; Raju, G. B. Adsorption of arsenate on synthetic goethite from aqueous solutions. *J. Hazard. Mater.* **2006**, *136*, 281.
(34) Gu, Z.; Fang, J.; Deng, B. Preparation and evaluation of GAC-based iron-containing adsorbents for arsenic removal. *Environ. Sci. Technol.* **2005**, *39*, 3833.
(35) Jang, M.; Shin, E. W.; Park, J. K.; Choi, S. I. Mechanisms of arsenate adsorption by highly-ordered nano-structured silicate media impregnated with metal oxides. *Environ. Sci. Technol.* **2003**, *37*, 5062.
(36) Lafferty, B. J.; Loeppert, R. H. Methyl arsenic adsorption and desorption behavior on iron oxides. *Environ. Sci. Technol.* **2005**, *39*, 2120.
(37) Seko, N.; Basuki, F.; Tamada, M.; Yoshii, F. Rapid removal of arsenic(V) by zirconium(IV) loaded phosphoric chelate adsorbent synthesized by radiation induced graft polymerization. *React. Funct. Polym.* **2004**, *59*, 235.
(38) Min, J. H.; Hering, J. G. Arsenate sorption by FE(III)-doped alginate gels. *Water Res.* **1998**, *32*, 1544.
(39) Li, Y. H.; Di, Z. C.; Ding, J.; Wu, D. H.; Luan, Z. K.; Zhu, Y. Q. Adsorption thermodynamic, kinetic and desorption studies of Pb^{2+} on carbon nanotubes. *Water Res.* **2005**, *39*, 605.
(40) Wang, J.; Xu, W.; Chen, L.; Jia, Y.; Wang, L.; Huang, X. J.; Liu, J. H. Excellent fluoride removal performance by CeO_2−ZrO_2 nanocages in water environment. *Chem. Eng. J.* **2013**, *231*, 198.